Biochimica et Biophysica Acta 1837 (2014) 750–760

Contents lists available at ScienceDirect

Biochimica et Biophysica Acta

journal homepage: www.elsevier.com/locate/bbabio

Evidence for interaction between the triheme cytochrome PpcA from *Geobacter sulfurreducens* and anthrahydroquinone-2,6-disulfonate, an analog of the redox active components of humic substances

Joana M. Dantas [a], Leonor Morgado [a], Teresa Catarino [b,c], Oleksandr Kokhan [d], P. Raj Pokkuluri [e], Carlos A. Salgueiro [a,*]

[a] Requimte-CQFB, Departamento de Química, Faculdade de Ciências e Tecnologia, Universidade Nova de Lisboa, Campus Caparica, 2829-516 Caparica, Portugal
[b] Instituto de Tecnologia Química e Biológica, Universidade Nova de Lisboa, Av. da República, 2780-157 Oeiras, Portugal
[c] Departamento de Química, Faculdade de Ciências e Tecnologia, FCT, Universidade Nova de Lisboa, 2829-516 Caparica, Portugal
[d] Chemical Sciences and Engineering Division, Argonne National Laboratory, Argonne, IL 60439 USA
[e] Biosciences Division, Argonne National Laboratory, Argonne, IL 60439 USA

ARTICLE INFO

Article history:
Received 15 November 2013
Received in revised form 4 February 2014
Accepted 6 February 2014
Available online 12 February 2014

Keywords:
AQDS
Geobacter
Humics
Multiheme cytochromes
NMR
Electron transfer

ABSTRACT

The bacterium *Geobacter sulfurreducens* displays an extraordinary respiratory versatility underpinning the diversity of electron donors and acceptors that can be used to sustain anaerobic growth. Remarkably, *G. sulfurreducens* can also use as electron donors the reduced forms of some acceptors, such as the humic substance analog anthraquinone-2,6-disulfonate (AQDS), a feature that confers environmentally competitive advantages to the organism. Using UV–visible and stopped-flow kinetic measurements we demonstrate that there is electron exchange between the triheme cytochrome PpcA from *Gs* and AQDS. 2D-^{1}H–^{15}N HSQC NMR spectra were recorded for ^{15}N-enriched PpcA samples, in the absence and presence of AQDS. Chemical shift perturbation measurements, at increasing concentration of AQDS, were used to probe the interaction region and to measure the binding affinity of the PpcA–AQDS complex. The perturbations on the NMR signals corresponding to the PpcA backbone NH and heme substituents showed that the region around heme IV interacts with AQDS through the formation of a complex with a definite life time in the NMR time scale. The comparison of the NMR data obtained for PpcA in the presence and absence of AQDS showed that the interaction is reversible. Overall, this study provides for the first time a clear illustration of the formation of an electron transfer complex between AQDS and a *G. sulfurreducens* triheme cytochrome, shedding light on the electron transfer pathways underlying the microbial oxidation of humics.

1. Introduction

Microbial extracellular electron transfer processes are currently explored for practical applications in the bioremediation and bioenergy fields. Extracellular electron transfer is one the most remarkable features of the species belonging to the *Geobacteraceae* family, by which these bacteria can reduce toxic or radioactive metals and convert renewable biomass into electricity [1,2]. *Geobacter metallireducens and Geobacter sulfurreducens* are examples of *Geobacteraceae* bacteria that are able to transfer electrons to extracellular metal oxides, such as Fe(III) or U(VI) [1,3–7]. Remarkably, these species can also use the reduced forms of these compounds as energy sources [8,9]. This versatility was also observed with electrode surfaces [1,5–7] and with the humic substance analog, anthraquinone-2,6-disulfonate (AQDS) [10,11]. Electrode surfaces and AQDS can be used by the bacterium *G. sulfurreducens* (*Gs*) as terminal electron acceptors, but it was also shown that *Gs* can use as electron donor either a negatively poised electrode or the reduced form of AQDS [12,13]. AQDS is commonly used to investigate bacterial humic respiration mechanisms [10,11]. Humic substances are natural organic matter formed by the decomposition of plant, animal, and microbial tissues, which are widely distributed in terrestrial and aquatic environments. All known humic-reducing microorganisms are capable of transferring electrons (and protons) to AQDS, reducing it to anthrahydroquinone-2,6-disulfonate (AH_2QDS) [10,14]. Gene knockout experiments carried out in *Gs* suggested that the humic (or AQDS) respiration uses multiple routes for electron transfer [15]. However, the actual molecular mechanisms or electron transfer pathways of respiration underlying the use of these compounds is presently unknown. Compared to microbial reduction of AQDS, less information is available on the use of AH_2QDS as electron donor. Several studies have demonstrated that different anaerobic bacteria can oxidize reduced humic substances, or analogs, in the

Abbreviations: PpcA, *Geobacter sulfurreducens* triheme cytochrome encoded by gene GSU0612; AQDS, anthraquinone-2,6-disulfonate; AH_2QDS, anthrahydroquinone-2,6-disulfonate (fully reduced AQDS)

* Corresponding author at: Departamento Química, Faculdade de Ciências e Tecnologia, Universidade Nova de Lisboa, Campus Caparica, 2829-516 Caparica, Portugal. Tel.: +351 212 948 300; fax: +351 212 948 385.
E-mail address: csalgueiro@fct.unl.pt (C.A. Salgueiro).

http://dx.doi.org/10.1016/j.bbabio.2014.02.004
0005-2728/

presence of suitable electron acceptors [12,16,17]. In this case, the organisms obtain carbon from other limited but readily degradable sources, such as acetate, and simply use AH_2QDS as an energy source [18]. This capability provides these organisms a potential competitive advantage over other heterotrophs that require organic compounds as both carbon and energy source and, therefore, need significantly higher concentrations of carbon compounds to grow [18].

Analysis of the fully sequenced *Gs* genome revealed a large number and diversity of *c*-type cytochromes [19]. The triheme cytochrome PpcA is highly abundant in the periplasm of *Gs* [20] and to date is the best characterized protein from all *Geobacteraceae*. PpcA contains 71 residues, harbors three covalently attached *c*-type hemes and has been structurally and functionally characterized in detail [20–28]. The crystal and the solution structures of PpcA were determined in the fully oxidized and fully reduced forms, respectively [22,25]. These structures revealed that the three heme groups are similarly arranged to tetraheme cytochrome c_3 (except for heme II and the corresponding fragment of the polypeptide chain, which are absent in PpcA) and have bis-histidinyl axial coordination [22,25]. Thus, to be consistent with the literature, the PpcA heme groups are numbered I, III and IV (Roman numerals indicate the heme in the order of attachment to the CXXCH motif in the polypeptide chain). The thermodynamic properties of PpcA showed that the three heme groups have different and negative reduction potentials, which cover the functional range −152 to −108 mV at pH 7.5 [26]. These potentials are strongly modulated by heme–heme interactions and by interactions with protonated groups (redox-Bohr effect), establishing a preferential electron transfer pathway coupled to proton transfer. This functional mechanism is achieved by the selection of specific redox states that the protein can access during the redox cycle and might be related to the formation of proton electrochemical potential gradient across the periplasmic membrane [26,28]. The mechanism that allows PpcA to perform such concerted e^-/H^+ transfer is driven by the protonation/deprotonation of a redox-Bohr center, which was assigned to the heme IV propionate 13 group (P^{IV}_{13}, according to the IUPAC Nomenclature) [22].

Since AH_2QDS can be used as electron donor by *G. sulfurreducens* and also couples e^-/H^+ transfer [15,29], in the present work we used UV–visible, stopped-flow kinetics and NMR measurements to investigate whether AH_2QDS and PpcA can function as redox partners and to fingerprint the regions involved in the interaction between these two molecules. The results of these experiments allowed us to present for the first time biochemical and biophysical evidence for a molecular interaction between PpcA and a putative redox partner, an important step for understanding the humic respiratory pathways in *G. sulfurreducens*.

2. Materials and methods

2.1. Expression and purification of triheme cytochrome PpcA

Uniformly ^{15}N-labeled and unlabeled PpcA were expressed in *Escherichia coli* as previously described [30]. Briefly, the PpcA gene was cloned in plasmid pCK32 and co-expressed with plasmid pEC86 that encodes for the cytochrome *c* maturation gene cluster [31] in *E. coli* BL21(DE3) cells. After reaching an OD_{600} of ~1.5, cultures were processed in either of two ways: (i) addition of 10 μM isopropyl β-D-thiogalactoside (IPTG) and growing overnight at 30 °C to express unlabeled protein, followed by a centrifugation step to harvest the cells; (ii) cells were collected by centrifugation, washed twice with 250 mL salt solution containing 3 g/L KH_2PO_4, 6 g/L Na_2HPO_4 and 0.5 g/L NaCl, resuspended in minimal media (in a ratio of 250 mL of minimal medium for each liter of 2× YT medium) supplied with 1 g/L $^{15}NH_4Cl$ as nitrogen source (together with 1 mM of the heme precursor α-aminolevulinic acid, trace amounts of metal ion salts, biotin and thiamine), grown overnight at 30 °C in the presence of 40 μM IPTG and harvested by centrifugation. Isolation of the periplasmic fraction and purification of the protein was done as previously described [30,32].

2.2. UV–visible and kinetic experiments

Electron exchange between AQDS and the triheme cytochrome PpcA was studied, in both directions, using UV–visible spectroscopy measurements at equilibrium and stopped-flow kinetics. Sample preparation and manipulations were performed at 25 °C under strict anaerobic conditions (O_2 level < 1 ppm) inside anaerobic glove chambers with argon circulation to avoid sample reoxidation. All electronic absorption spectra were acquired between 290 nm and 650 nm, using an Evolution 300 UV–vis Spectrophotometer (Thermo Fisher Scientific) equipped with a Fiber Optic Coupler and fiber optics inside an MBraun LABstar anaerobic chamber. Rapid mixing kinetic experiments were carried out on a HI-TECH Scientific SF-61 DX2 stopped-flow instrument inside an anaerobic chamber Mbraun MB 150 I. The data were acquired with a diode array in the wavelength range 350 nm to 700 nm.

Samples were prepared in phosphate buffer pH 7.1 with NaCl (100 mM final ionic strength). The buffer was prepared inside the anaerobic chamber with degassed water. The protein solution (3 μM) was prepared by dilution of a stock solution in degassed buffer and the exact concentration was determined from the absorbance of the reduced PpcA at $\lambda = 552$ nm using an extinction coefficient of 97 500 $M^{-1}\ cm^{-1}$, recalculated from the value previously reported by Seeliger and coworkers [24,33]. A concentrated AQDS (≥98% purity, Sigma) stock solution (120 μM) was prepared in degassed buffer inside the anaerobic chamber and the 30 μM, 6 μM, 3 μM, and 1.5 μM AQDS solutions were prepared by successive dilutions of the concentrated stock solution. Reduced solutions of AH_2QDS and PpcA were obtained by adding a stoichiometric amount of sodium dithionite, after determining the concentration of the sodium dithionite solution from its absorbance at $\lambda = 315$ nm using an extinction coefficient of 8000 $M^{-1}\ cm^{-1}$ [34]. UV–visible spectra were acquired before and after addition of sodium dithionite to monitor the efficiency of the reduction and to confirm that there is no excess reducing agent in the solution. In the reductive experiments, oxidized PpcA was mixed with AH_2QDS in the stopped-flow apparatus and the reduction of the cytochrome was followed in the full spectral range (350–700 nm) at two different timescales (0.15 and 1.5 s). To obtain the observed rate constants for the reduction of the cytochrome by AH_2QDS, the time dependence of the signal at $\lambda = 552$ nm was fitted with one or two exponentials as necessary. In the oxidative experiments reduced PpcA was mixed with oxidized AQDS in stopped-flow apparatus and the oxidation of the cytochrome was followed in the full spectral range (350–700 nm) at three timescales (0.15, 0.75 and 1.5 s). To obtain the observed rate constants for the oxidation of the cytochrome by the AQDS, the time dependence of the signal at $\lambda = 552$ nm was fitted with one or two exponentials. The following cytochrome to quinone ratios: 1:0.5, 1:1, 1:2, 1:10 and 1:40 were used in both types of experiments. Because the reaction is very fast, part of it is lost in the dead time (3 ms) of the apparatus. Thus, the level of reduction of the first spectrum was determined from spectral deconvolution using standard spectra for the fully oxidized and fully reduced forms.

2.3. NMR studies

2.3.1. NMR samples preparation and experiments

For NMR studies, samples of PpcA cytochrome (~0.5 mM) were prepared in phosphate buffer pH 7.1 with NaCl (100 mM final ionic strength) in 92%H_2O/8%^2H_2O (^{15}N-labeled sample) or pure ^2H_2O (unlabelled sample). The NMR experiments were acquired in a Bruker Avance III 600 spectrometer equipped with a triple-resonance cryoprobe (TCI) at 25 °C. ^1H chemical shifts were calibrated using the water signal as internal reference and the ^{15}N chemical shift calibrated through indirect referencing [35]. Spectra were processed using software TOPSPIN (Bruker Biospin, Karlsruhe, Germany) and analyzed with program Sparky (TD Goddard and DG Kneller, Sparky 3, University of California, San Francisco, USA). The following set of experiments was acquired for cytochrome PpcA in presence of AQDS: ^{15}N- labeled

sample: 2D-^{1}H–^{15}N HSQC (heteronuclear single quantum coherence); unlabeled sample in pure ^2H_2O: 2D-^{1}H–^{13}C HSQC, 2D-^{1}H–^{1}H-TOCSY (total correlation spectroscopy) with 45 ms mixing-time and 2D-^{1}H–^{1}H-NOESY (nuclear Overhauser effect spectroscopy) with 80 ms mixing-time. 1D-^{1}H NMR spectra were obtained before and after each multidimensional spectrum to confirm protein integrity. The effect of humic substance analog on the chemical shifts of PpcA backbone NH signals was monitored by the analysis of a series of 2D-^{1}H–^{15}N HSQC spectra in the presence of increasing amounts of AQDS. The pH of the sample was measured before and after each series to confirm that pH of the solution is maintained. To measure the impact of the interaction also on the AQDS NMR signals, 1D-^{1}H NMR spectra of AQDS in the presence and absence of PpcA were acquired.

To investigate the binding reversibility between PpcA and AQDS, 1D-^{1}H NMR spectra were acquired for PpcA in the absence of AQDS and after removal of this molecule by ultrafiltration methods (Amicon Ultra, 3k Da). All 1D-^{1}H NMR spectra in the present study were acquired by collecting 64K data points with at least 64 scans.

2.3.2. Assignment of the NMR signals

The PpcA backbone NH signals and heme proton signals were previously assigned at 25 °C and pH 5.5 [36]. In the present work these signals were re-assigned at 25 °C and pH 7.1 using the methodologies previously described [22] and then used to monitor the AQDS-induced chemical shift perturbations.

2.4. Determination of interaction sites

The general theoretical framework used to fingerprint the interacting region(s) between PpcA and AQDS was previously described by Schumann and co-workers [37] and can be sketched as follows. The weighted average chemical shift ($\Delta\delta_{comb,j}$) of each backbone NH signal was calculated according to Eq. (1)

$$\Delta\delta_{comb,j} = \sqrt{(\Delta\delta_H)^2 + (w_i\Delta\delta_N)^2}, \quad (1)$$

where $\Delta\delta_H$ is the chemical shift change in ppm in ^{1}H dimension, $\Delta\delta_N$ is the chemical shift change in ppm in ^{15}N dimension and the term $w_i = |\gamma^{15}N|/|\gamma^1H|$ compensates for the scaling differences between ^{15}N and ^{1}H chemical shifts [37]. To select the most affected signal(s) to be used in the calculation of the equilibrium dissociation constant (K_d), a cut-off value was determined iteratively with the standard deviation to zero value, σ_0^{corr}, according to Eq. (2) [37]

$$\sigma_0^{corr} = \sqrt{\frac{1}{N}\sum\left(\Delta\delta_{comb,j} - 0\right)^2}, \quad (2)$$

where N corresponds to the number of $\Delta\delta_{comb}$ values determined. Briefly, in an initial step a value of σ_0 is determined from all $\Delta\delta_{comb}$ values. The $\Delta\delta_{comb}$ exceeding three times the determined σ_0 are removed and a first corrected standard deviation σ_0^{corr} is obtained for the remaining $\Delta\delta_{comb}$ values. If there are $\Delta\delta_{comb}$ values larger than three times the new σ_0^{corr} value, they will be excluded and a new σ_0^{corr} will be determined. This process is repeated until no $\Delta\delta_{comb}$ value larger than three times that of the actual σ_0^{corr} remained, which is then taken as the cut-off criterion. The binding curves for the interaction between the protein P (PpcA) and the ligand L (AQDS) were obtained by plotting the magnitude of the chemical shift change ($\Delta\delta_{comb}$) as function of AQDS concentration. The data were fitted using the tool Solver from Microsoft Excel with $\Delta\delta_{comb}$ and [ADQS] as dependent and independent variables, respectively and the dissociation constant (K_d) and $\Delta\delta_{max}$ as the fit parameters considering fast exchange conditions at the binding site, according to the following equilibrium: P + L ↔ PL (Eq. (3))

$$\Delta\delta_{comb,j} = (\Delta\delta_{max})\frac{([P] + [L] + K_d) - \sqrt{([P] + [L] + K_d)^2 - 4[P][L]}}{2[P]}. \quad (3)$$

In Eq. (3) $\Delta\delta_{max}$ is the maximum chemical shift change, [P] the total protein concentration and [L] the total ligand concentration.

2.5. Docking calculations

Docking calculations were performed with Anchor-and-Grow algorithm as implemented in DOCK 6.4 [38]. Atomic coordinates of PpcA were taken from the NMR structure of the protein (PDB: 2LDO). Atomic coordinates for AH_2QDS were taken from LUPBUT entry of the Cambridge Structural Database. Protein and ligand structures were prepared for docking calculations with UCSF Chimera 1.5.2 [39]. Hydrogens were added to protein to reflect the neutral pH and heme charges are that for an oxidized state from AMBER force field.

3. Results

3.1. Equilibrium and kinetic studies probed by UV–visible spectroscopy

The different UV–visible absorption spectral signatures were used to investigate the extent to which PpcA was reduced by AH_2QDS or oxidized by AQDS at equilibrium. The UV–visible absorption spectra of PpcA display the typical features of a hexacoordinated *c*-type cytochrome containing hemes in the low spin state (Fig. 1A). In the oxidized form the spectrum is dominated by the Soret band with a maximum at 406 nm. After reduction with sodium dithionite, three bands are observed at 417 nm (Soret band), 522 nm (β band) and 552 nm (α band), typical of low-spin ferrous *c*-type hemes. On the other hand, the UV–visible absorption spectrum of AQDS displays an absorption band with a maximum at 325 nm, whereas that of AH_2QDS shows two bands with maxima at 385 nm and 410 nm (Fig. 1B). In the present work we firstly monitored by UV–visible spectroscopy the effect of the addition of an oxidized PpcA ($PpcA^{ox}$) sample to a solution containing AH_2QDS (Fig. 2A) and the reverse experiment by adding AQDS to a sample of reduced PpcA ($PpcA^{red}$) (Fig. 2B). The UV–visible spectra obtained after the addition of an equimolar amount of $PpcA^{ox}$ to a solution containing AH_2QDS showed the features of reduced cytochrome, as confirmed by the typical α and β bands (see blue line in Fig. 2A). In the UV–visible spectrum of AH_2QDS before addition of $PpcA^{ox}$ (dashed line in Fig. 2A), the typical band of sodium dithionite, with an absorption maximum at 315 nm, is not present, confirming that reduction of PpcA is achieved only via oxidation of AH_2QDS. Although the features of the reduced form are present, it is important to stress that the cytochrome is not fully reduced, neither could it be, because the equimolar concentration of redox partners does not correspond to an equimolar concentration of electrons, since the reduced quinone is a two electron donor whereas the oxidized cytochrome needs three electrons to become fully reduced. In fact, the value of the absorbance at 552 nm shows that the PpcA is less than 50% reduced in this experiment. In the reverse experiment, the addition of equimolar AQDS to $PpcA^{red}$, results in only ca. 20% of oxidation of the cytochrome, and even after the addition of a 40× molar excess of AQDS, the percentage of oxidation of the cytochrome is not larger than 50%, as shown by the UV–visible spectra (see blue lines in Fig. 2B). These results show that, at equilibrium, the electron transfer occurs preferentially from the reduced quinone to the oxidized cytochrome, as expected on the basis of their reduction potentials. The stopped-flow technique was used to obtain kinetic information on the reaction between reduced quinone and $PpcA^{ox}$, and on the reverse reaction, between oxidized quinone and $PpcA^{red}$. Both types of experiments were carried out for different cytochrome to

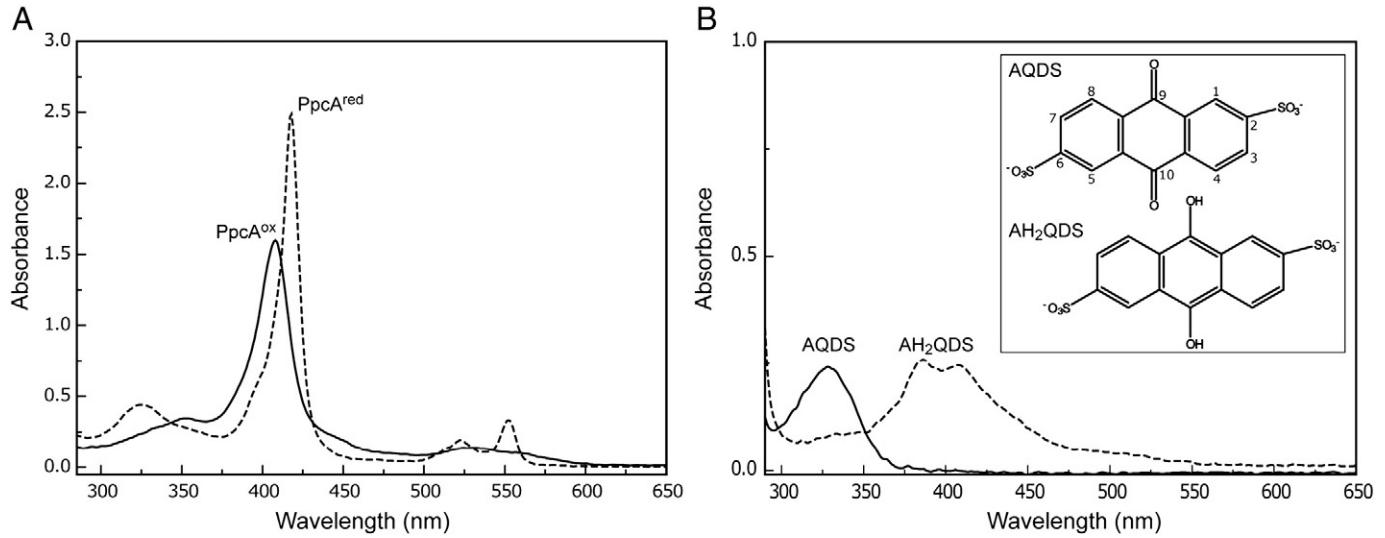

Fig. 1. UV–visible absorption spectra of PpcA (A) and AQDS (B). The continuous and dashed lines correspond to the oxidized and reduced forms, respectively. The spectra were obtained at 25 °C and pH 7. The concentration of PpcA and AQDS were 3 μM and 31 μM, respectively. Structures of AQDS and AH_2QDS are indicated in the inset and were drawn with program ChemDraw Ultra 12.0 [52].

quinone molar ratios. Normalized kinetic traces for the reductive and oxidative experiments are presented in Fig. 2C and D, respectively, and the result of the fit of the data with single exponentials is shown in Table 1. Up to 1:2 cytochrome to quinone ratio, the observed rate constants are constant, and very similar for the reductive and oxidative experiments: $k_{obs} \approx 70\ s^{-1}$. For the larger ratios, 1:10 and 1:40, the observed rate constant increases in an approximately linear fashion and the amplitudes, which were increasing with increasing ratios, tend to stabilize. In the reductive experiments, a slow phase ($k_{obs} \approx 1\ s^{-1}$) with significant amplitude (>10% of the total reaction) seems to be associated with the transfer of the third electron, leading to the full reduction of the protein. In the oxidative experiments a slow phase ($k_{obs} \approx 3\ s^{-1}$) is also visible, but it does not seem so significant, possibly because oxidation never progresses beyond 64%. The extent of the overall reaction, observed both in the reductive and in the oxidative kinetic experiments, is in good agreement with the results obtained in the UV-visible equilibrium experiments, confirming that thermodynamic equilibration is reached in a short time scale.

3.2. PpcA-AQDS interaction probed by NMR

Multidimensional isotope edited-NMR spectroscopy is a powerful technique to probe conformational changes in the chemical environment of a nucleus and has been used to study redox complexes, providing a wealth of information about the nature of complex interfaces. Complex formation gives rise to changes in the chemical environment of the nuclei at the interface, such that their chemical shift (δ) differs in the bound and free forms. However, the study of molecular interactions involving heme proteins is complicated by the significant differences in the NMR spectra of their reduced and oxidized forms. To overcome this effect, the analysis at the atomic level of the interacting regions in electron transfer complexes is typically carried out with both partners in the same oxidation state. There are plenty of examples in the literature that illustrate the power of this approach for obtaining physiological and structural insights into the details of interactions between redox partners [40–43]. The above scenario also applies to cytochrome PpcA, which is diamagnetic in the reduced form ($S = 0$) and paramagnetic in the oxidized form ($S = 1/2$). Therefore, the unpaired electron of each heme iron exerts significant paramagnetic shifts on the heme signals and nearby residues, yielding different NMR spectra. Consequently, the same type of signal is differently affected by the paramagnetic centers, showing different levels of broadness and are spread all over the entire NMR spectral window (for a review see [36]). To illustrate this effect the 2D-^{1}H–^{15}N HSQC NMR spectra obtained for $PpcA^{red}$ and $PpcA^{ox}$ are indicated in supplementary Fig. S1.

In the present work, the molecular interactions between cytochrome PpcA and AQDS were first investigated by measuring the chemical shift perturbation on the backbone NH signals of $PpcA^{ox}$. All NH signals were assigned at pH 7.1, except for residues Ala^1, Asp^2, Gly^{36}, Gly^{42}, Lys^{49} and Cys^{51}. The backbone NH signals at the N-terminal residues are usually not observable due to the inherent flexibility of this region. The backbone NH signals of Gly^{36} and Gly^{42} were not observable, most probably due to signal broadness caused by the nearby hemes I and IV paramagnetic iron atoms, since they were not detected also at low pH values. On the other hand, the backbone amide signals of Lys^{49} and Cys^{51} were not observed due to their rapid solvent exchange at pH 7.1. The chemical shift perturbations on the backbone NH signals of $PpcA^{ox}$ with increasing amounts of AQDS were monitored by recording a series of 2D-^{1}H–^{15}N HSQC NMR spectra (Fig. 3). The NH signals showing highest chemical shift perturbation are those in the polypeptide segment Asn^{10} to Val^{13}, Lys^{43}, Glu^{44}, Ala^{46}, Lys^{52}, Cys^{65} and Lys^{70}, all residues located near heme IV with one exception of residue Cys^{27} which is near heme I. Analysis of the chemical shift perturbation as a function of AQDS concentration yielded hyperbolic binding curves which were fitted to a 1:1 model considering fast exchange conditions (Fig. 4). As shown by the equilibrium and kinetic studies probed by UV–visible spectroscopy, $PpcA^{ox}$ can be fully reduced in the presence of AH_2QDS. However, the three heme groups of PpcA provide three distinct entry gates for the electrons. Therefore, it is expected that the donor and at least one of the heme groups of PpcA are in close proximity for an effective electron transfer. Under this scenario, we then moved to study the effect of the interaction between AQDS and the $PpcA^{ox}$ on the heme group NMR signals. PpcA is one of the smallest *c*-type cytochromes described so far with a high ratio of hemes to amino acids (approximately 1 heme per 24 amino acids). Thus, any perturbation caused by the binding of an extraneous molecule to PpcA is expected to affect the NMR signals of the heme substituents. Each heme has four heme methyls and their ^{1}H NMR signals are found in less crowded regions of the 1D-^{1}H NMR spectrum of $PpcA^{ox}$. For this reason, they constitute excellent probes for monitoring the chemical shift perturbations on $PpcA^{ox}$ heme groups. Consequently, in the present work the interactions between AQDS and $PpcA^{ox}$ were further evaluated by monitoring the chemical shift perturbation on the $PpcA^{ox}$ heme methyl signals on the 1D-^{1}H NMR spectra.

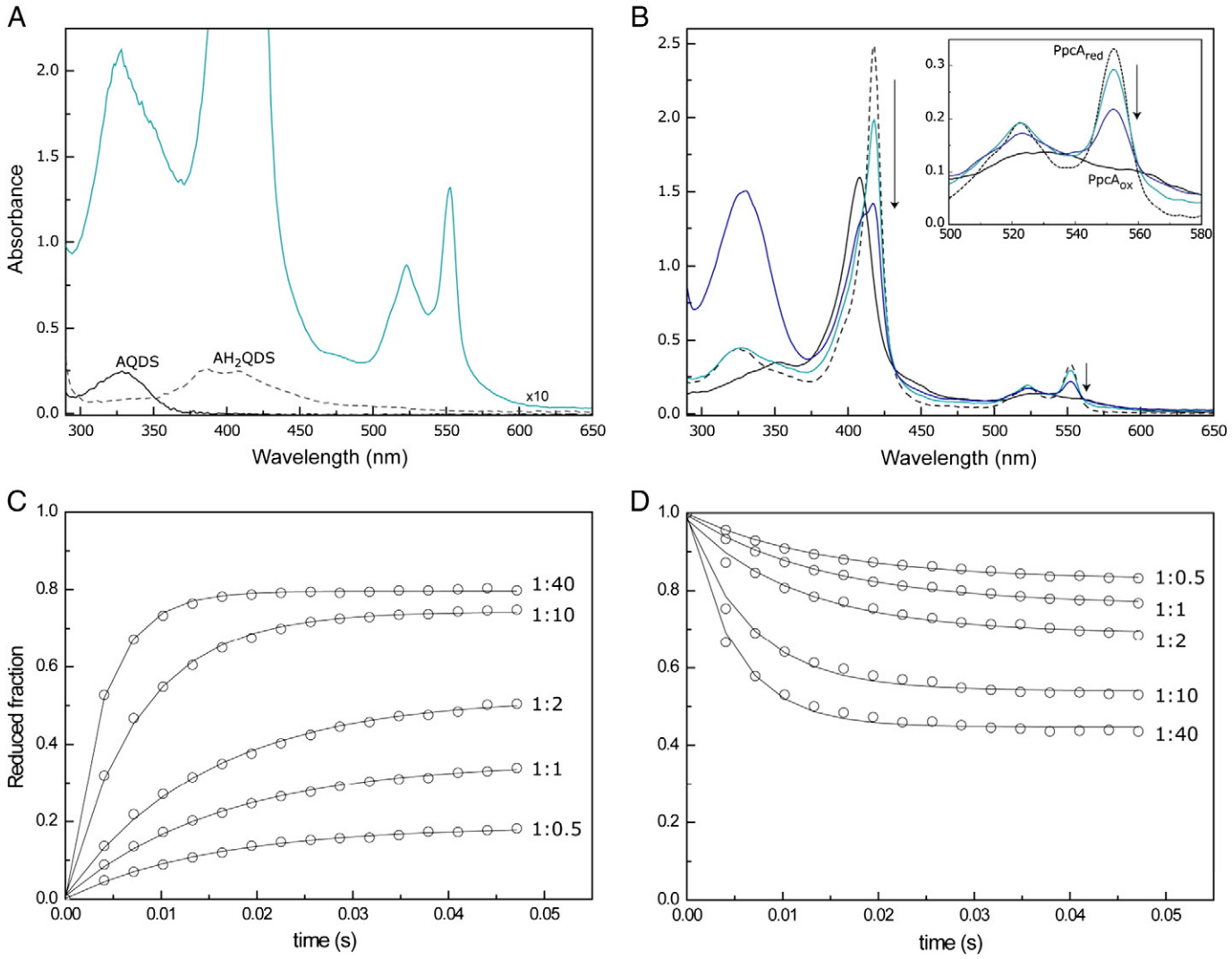

Fig. 2. Assays of AH_2QDS oxidation coupled to PpcA reduction (left panels) and AQDS reduction coupled to PpcA oxidation (right panels) at 25 °C and pH 7. (A) UV-visible spectra of AQDS (continuous black line) and AH_2QDS (dashed line). As an example the spectrum obtained for a ratio $PpcA^{ox}$:AH_2QDS 1:1 is indicated (continuous blue line) in this experiment the concentrations were both 3 μM. (B) UV-visible spectra of $PpcA^{ox}$ (continuous black line) and $PpcA^{red}$ (dashed black line). As an example the spectra obtained for $PpcA^{red}$:AQDS ratios of 1:1 and 1:40 are indicated by blue lines. In these experiments the concentration of PpcA was 3 μM and the concentration of AQDS was varied. The arrow points to increasing concentrations of AQDS. In the inset an enlarged scale of the spectra between 500 nm and 580 nm is showed for clarity. Panels (C) and (D) represent the fast electron transfer between AH_2QDS and $PpcA^{ox}$ and between $PpcA^{red}$ and AQDS, respectively. The traces were recorded at $\lambda = 552$ nm and normalized using the absorbance of the fully reduced and the fully oxidized cytochrome at the same wavelength. The time scale was corrected for the dead time of the stopped-flow apparatus. Cytochrome to quinone molar ratios of 1:0.5, 1:1, 1:2, 1:10 and 1:40 were used in both reductive (panel C) and oxidative (panel D) experiments. The solid lines are the result of the fit of the data with a single exponential, using the tool Solver from Microsoft Excel. The final concentration of protein was 3 μM in all experiments.

The low-field regions of the 1D-^{1}H NMR spectra, acquired during the titration of $PpcA^{ox}$ with increasing amounts of AQDS, are indicated in Fig. 5. The analysis of the chemical shift perturbation clearly shows that signals of heme IV methyls are the most affected (Fig. 5). The interaction between $PpcA^{ox}$ and AQDS was further investigated by observing the pattern of the AQDS signals in the 1D-^{1}H NMR spectra in the absence and presence of the protein (Fig. 6). The 1D-^{1}H NMR spectrum of free AQDS (Fig. 6A) shows three signals at 8.43, 8.16, 8.13 ppm

Table 1
Result of the fit of single exponential curves to the electron transfer data obtained in the stopped-flow experiments after normalization. The values for the percentage of total reduction and total oxidation were calculated from deconvolution of the last spectra, recorded in the longer time scale (1.5 s), using standard spectra for the fully reduced and fully oxidized states. The concentration of PpcA was 3.0 μM in all experiments. The data was acquired at 25 °C and pH 7.

PpcA reduction				PpcA oxidation			
[AH_2QDS] (μM)	Fast phase (%)	k_{obs} (s^{-1})	Total reduction (%)	[AQDS] (μM)	Fast phase (%)	k_{obs} (s^{-1})	Total oxidation (%)
1.5	18	65	18	1.5	17	69	18
3.0	35	61	36	3.0	23	69	26
6.0	51	68	56	6.0	29	85	35
30	74	131	>85	30	45	149	49
120	79	261	>95	120	55	198	64

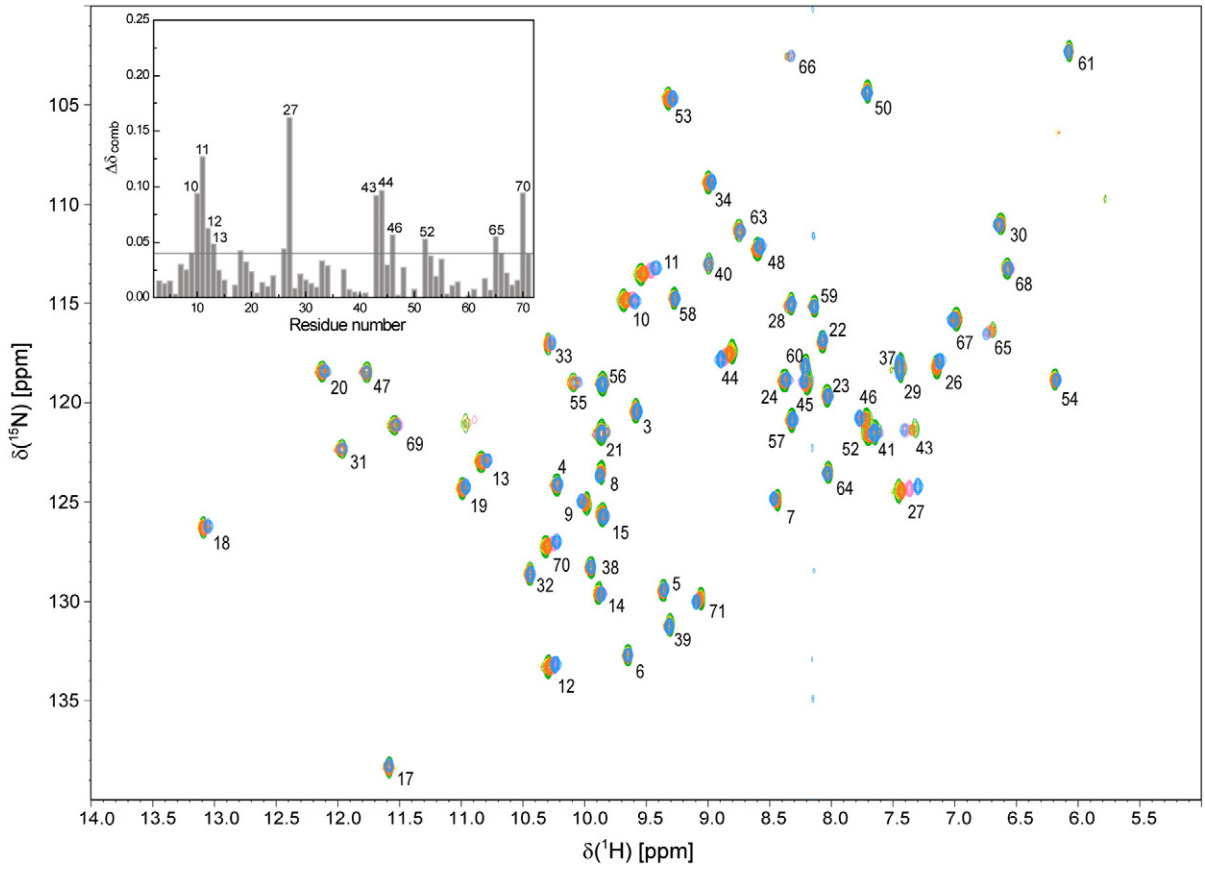

Fig. 3. Overlay of the 2D-^{1}H–^{15}N HSQC NMR spectra of ^{15}N-enriched PpcA^{ox} (0.5 mM) in the presence of increasing amounts of AQDS. The contours of the signals in the reference spectrum are shown in green while in the spectral overlay, the concentration of AQDS increases from green to blue contours. To clarity of the figure, only the spectra acquired with 0.8; 4.0; 15.8 and 39.6 mM AQDS are shown. The assignments of NH signals are indicated. The insets show the plot of the combined chemical shift changes determined from the directly observed ^{1}H and ^{15}N chemical shifts, according to the Eq. (1). The horizontal line in the inset was determined with the standard deviation to zero value, σ_0^{corr} (see Materials and methods).

that correspond to the three pairs of equivalent protons (H1/H5; H3/H7; H4/H8). The protons H1/H5 are considerably less shielded compared to the other pairs due to the electron-withdrawing effect of the sulfonate ion and correspond to the signal at 8.43 ppm. The two very close doublets centered at 8.16 and 8.13 ppm were assigned to the pairs of protons H3/H7 and H4/H8, respectively. In the presence of the protein, the pattern of AQDS signals is clearly affected, confirming the interaction between PpcA^{ox} and AQDS (cf. spectra expansions A and B in Fig. 6). Finally, the comparison of 1D-^{1}H NMR spectra of PpcA^{ox} obtained before and after removal of the ligand by ultrafiltration methods confirm that the interaction between the cytochrome and AQDS is fully reversible (Supplementary Fig. S2).

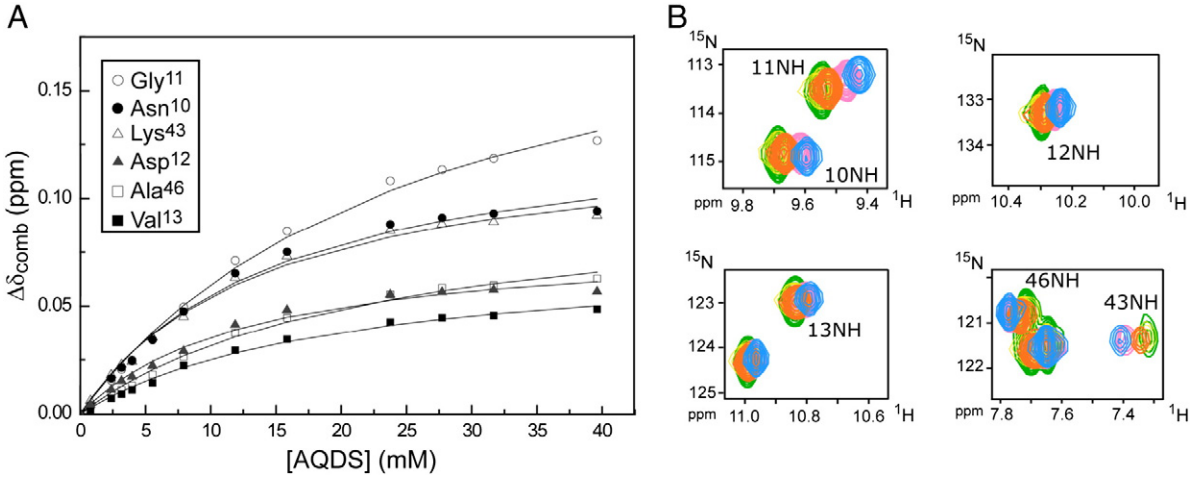

Fig. 4. Binding isotherms for PpcA^{ox}-AQDS interaction (A) and selected regions from overlaid 2D-^{1}H–^{15}N HSQC NMR spectra (B). In panel A, labels indicate the NH signals that were monitored in the chemical shift perturbation experiments (for clarity of the figure NH signals of Glu^{44}, Lys^{52}, Cys^{65} and Lys^{70} are not shown). Each data set was fit to a 1:1 binding model considering fast exchange conditions (solid lines). An average K_d value was calculated as 17.8 ± 5 mM from the titration curves. In the expansion of each NMR spectrum (panel B) the amount of AQDS increases from green to blue contours.

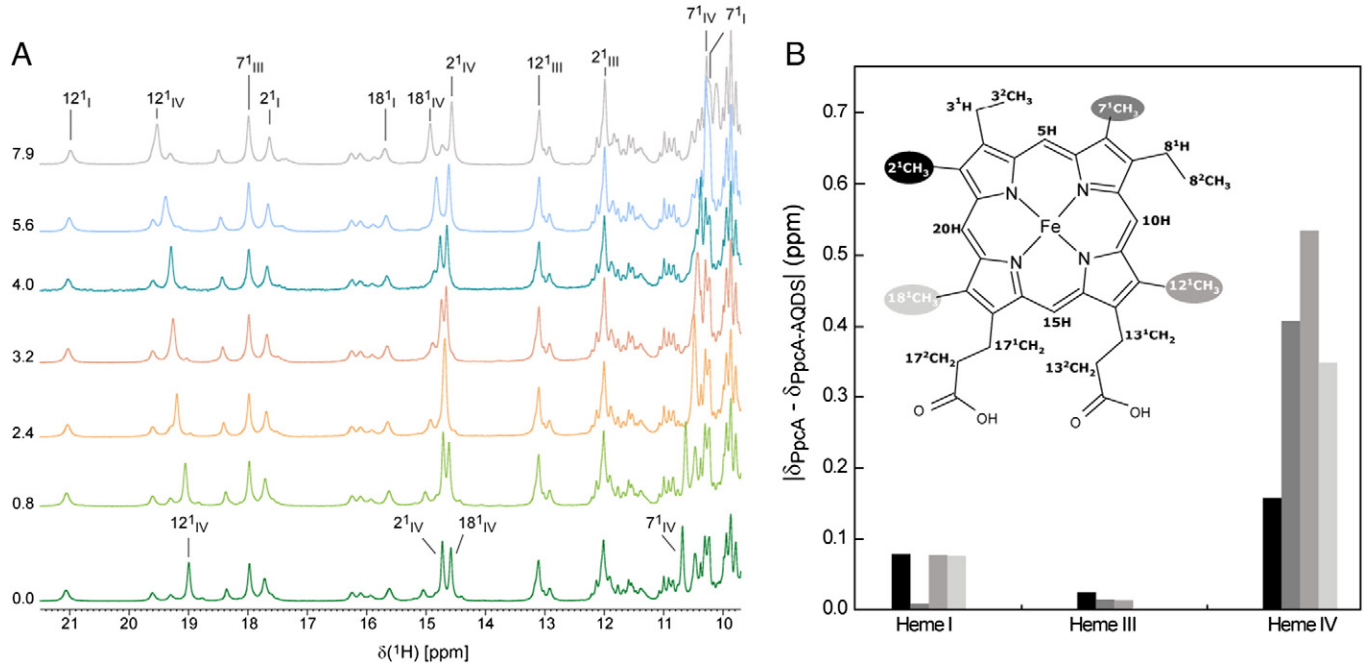

Fig. 5. ^{1}H chemical shift changes of the heme methyls of PpcA^{ox}. (A) Expansions of the low-field region of 1D-^{1}H NMR spectra obtained for PpcA^{ox} in presence of increasing amounts of AQDS. The heme methyl signals ($2^{1}CH_3$, $7^{1}CH_3$, $12^{1}CH_3$ and $18^{1}CH_3$) following the IUPAC nomenclature [53] are labeled, except heme methyl $18^{1}CH_3^{III}$ whose signal appears at a chemical shift of approximately 1 ppm. The value of AQDS concentration (mM) used in each experiment is indicated on the left of each spectrum. (B) Variation of the heme methyl group chemical shifts $|\delta_{PpcA}-\delta_{PpcA\,+\,AQDS}|$. The shifts were taken from the PpcA spectra obtained in the absence (δ_{PpcA}) and in the presence of 7.9 mM AQDS ($\delta_{PpcA\text{-}AQDS}$). The bars represent the ^{1}H chemical shift variations of methyl groups in the following order from left to right: $2^{1}CH_3$, $7^{1}CH_3$, $12^{1}CH_3$ and $18^{1}CH_3$. The diagram of a heme *c* is shown in the inset.

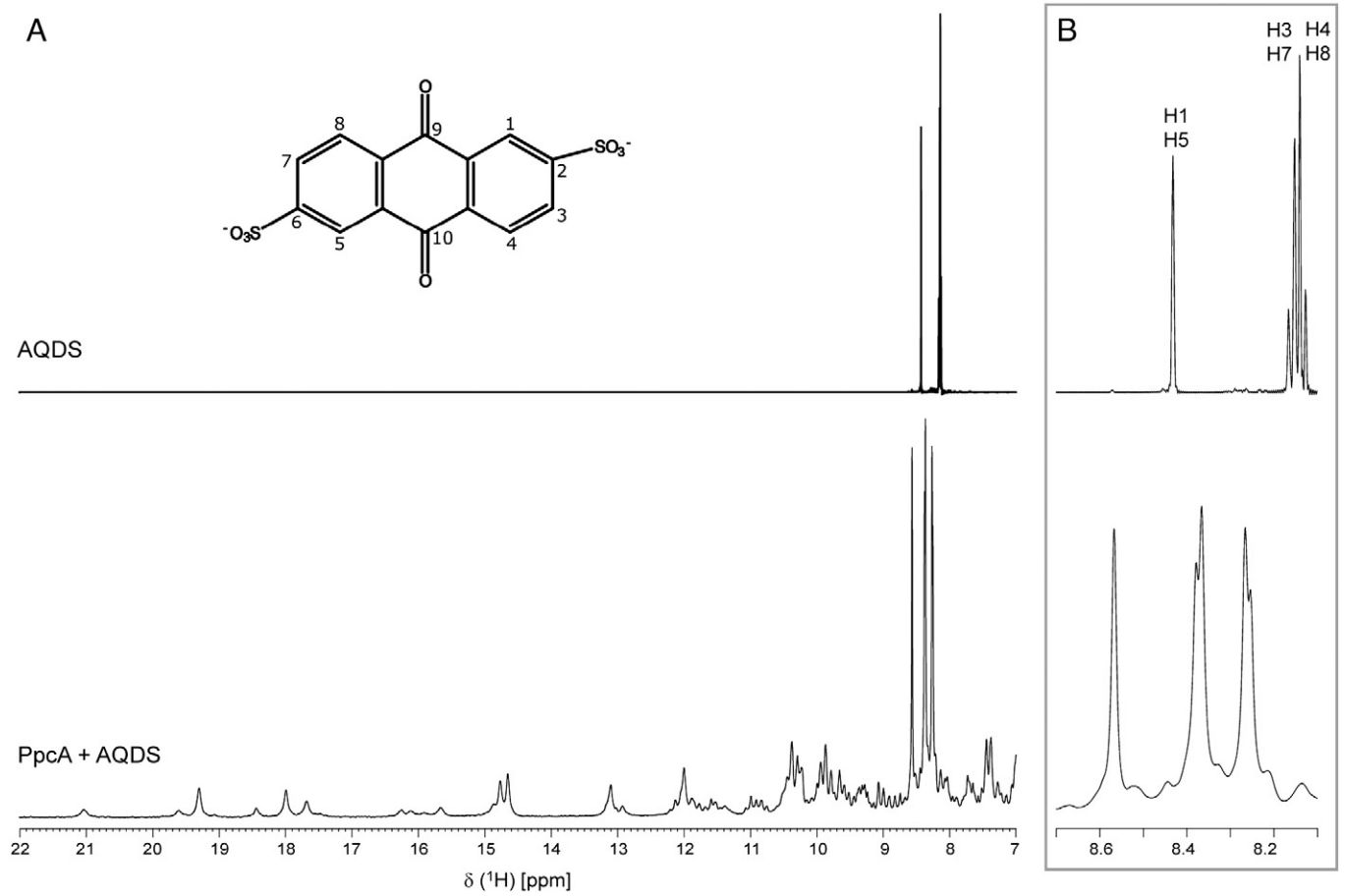

Fig. 6. ^{1}H chemical shift changes of the AQDS signals in presence of PpcA^{ox}. (A) 1D-^{1}H NMR spectral features of free AQDS (upper spectrum) and AQDS in the presence of PpcA^{ox} (lower spectrum). (B) Expansion of the spectral region containing the proton signals of AQDS. The three pairs of equivalent protons (H1/H5; H3/H7 and H4/H8) are indicated.

3.3. PpcA-AH_2QDS interaction probed by docking calculations

Docking was performed using the Anchor-and-Grow algorithm, implemented in Dock6.4 for binding of AH_2QDS to $PpcA^{ox}$. This model assumes that protein is rigid but the ligand may have some flexibility, which in the case of AQDS is only rotational flexibility of the sulfonate groups. Remarkably, the docking results showed that AH_2QDS binds near heme IV in six of the top ten complex models and mapped most residues showing significant NMR chemical shift perturbations (cf. Figs. 7 and 8).

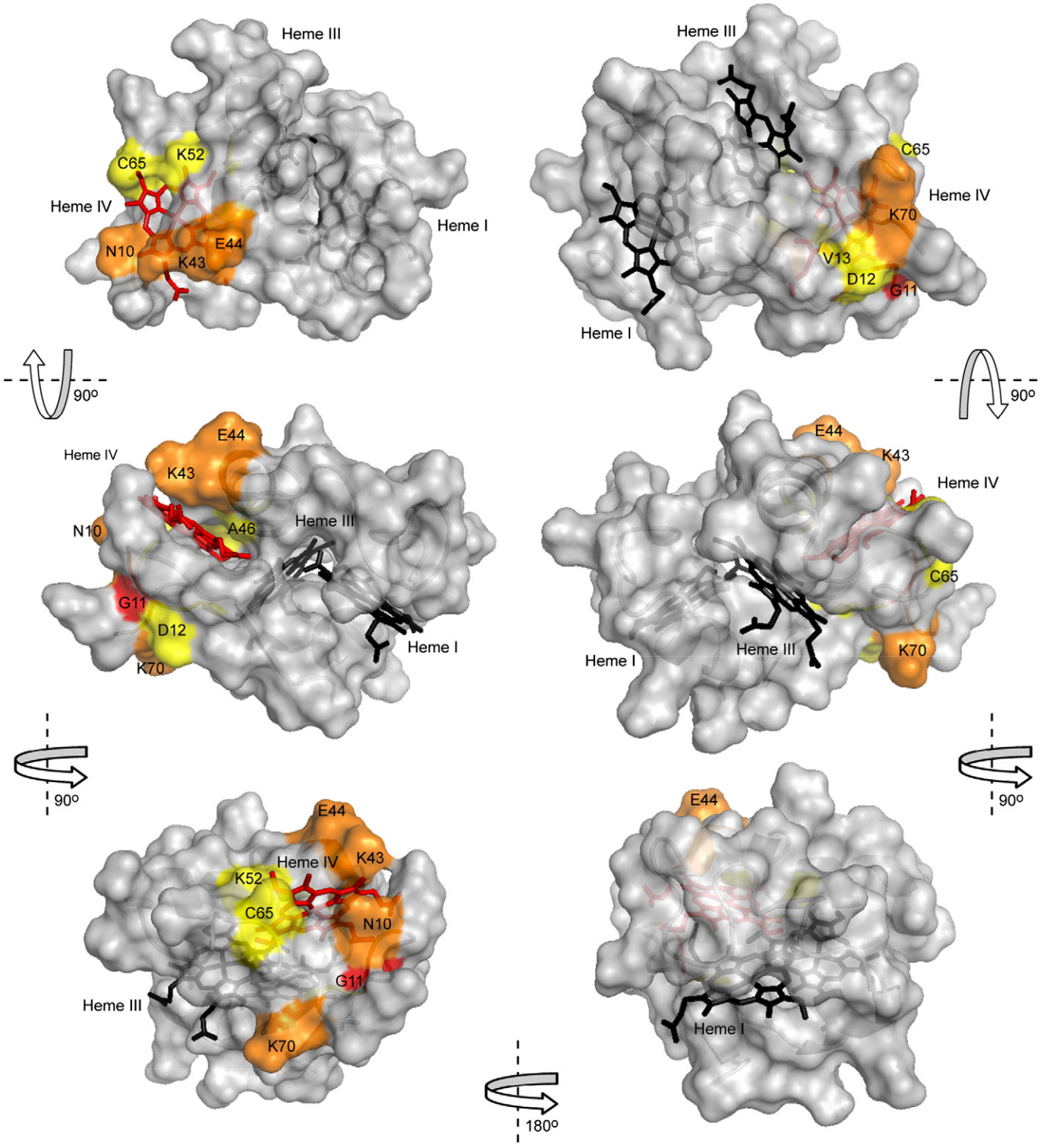

Fig. 7. Surface map of significantly perturbed residues in PpcA upon AQDS binding. The molecular surface was generated in PyMOL [54] by using the PpcA structure (PDB code, 2LDO [22]). Residues for which the amide resonances experienced small ($\Delta\delta_{comb} > 0.04$ ppm), medium ($\Delta\delta_{comb} \geq 0.07$ ppm) or large ($\Delta\delta_{comb} \geq 0.10$ ppm) shifts are colored yellow, orange and red, respectively. Heme IV is shown in red and hemes I and III are shown in black. The left and right panels are related by a 180° rotation. Upper images are related to lower images by 90° rotations as indicated.

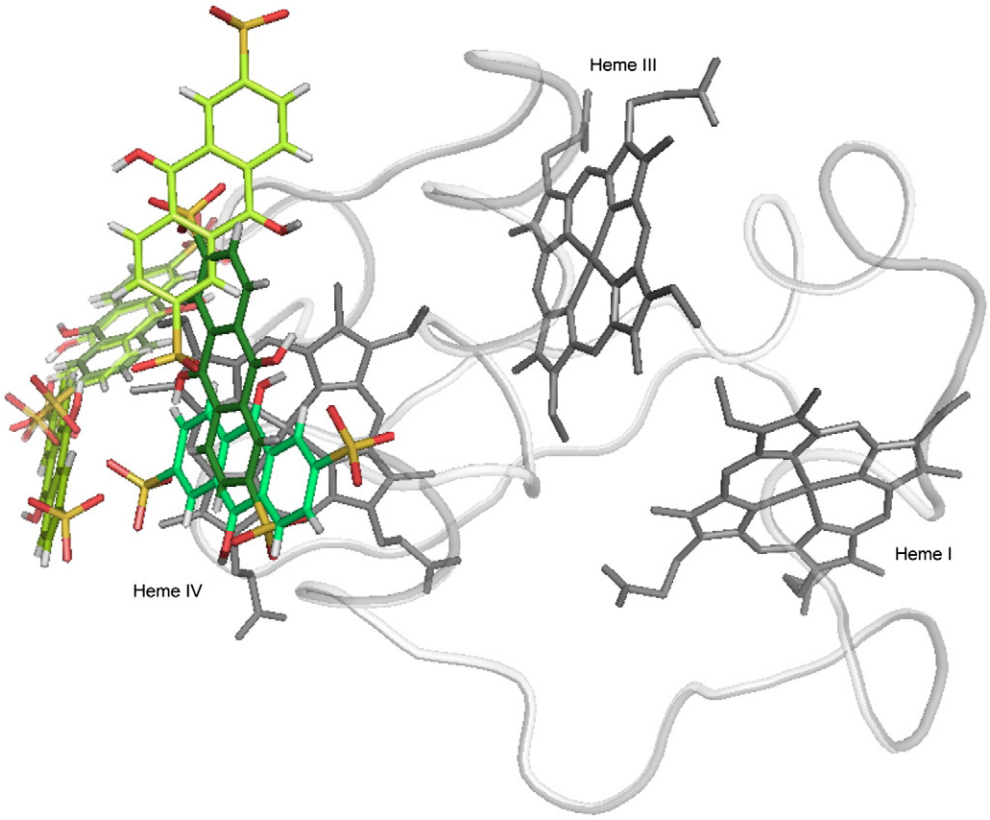

Fig. 8. PpcA–AH_2QDS docked complexes calculated in DOCK 6.4 [38]. PpcA (oriented as in the first panel of Fig. 7) is illustrated as a ribbon diagram with the heme groups shown in gray sticks. The six of the top 10 docking results for quinone binding near heme IV are shown.

4. Discussion

Previous studies have shown that the bacterium *G. sulfurreducens* can grow on carbon-limited sources using the electron donor AH_2QDS as energy source [12]. In addition, proteomic studies showed that PpcA is highly abundant in the periplasm of *Gs* [20,44]. Thus, in the present work, we used UV–visible spectroscopy and stopped-flow kinetics to investigate the rate in each direction of the electron-flow between AQDS and PpcA, and NMR spectroscopy to probe interaction regions between the two molecules. The kinetic data show that electron transfer proceeds in both directions at a similar rate but its extent is thermodynamically controlled, being more favorable in the case of the reduction of the cytochrome by the quinone (Table 1). In fact, the results obtained are consistent with the reduction potential values of these species at pH 7. The reduction potential of AH_2QDS is −184 mV [45] and that of PpcA is −117 mV [21], which thermodynamically favors the reduction of the latter. The analysis of the chemical shift perturbations on the $PpcA^{ox}$ backbone NH and heme methyl NMR signals enabled us to map the interaction region of the AQDS–PpcA redox complex to be in the vicinity of heme IV. This interaction was further confirmed by the spectral changes on the NMR pattern of AQDS signals in the presence of $PpcA^{ox}$ (Fig. 6). The broadness and displacement observed in the AQDS signals clearly confirmed the existence of a molecular interaction between the protein and the quinone.

The increasing chemical shift perturbations, as a function of AQDS concentration, indicated that the free and bound forms of cytochrome $PpcA^{ox}$ are in fast exchange on the NMR time scale. Of the 11 NH signals that exhibited significant chemical shift perturbation, 10 are located on the surface of the PpcA molecule in polypeptide regions that enwrap heme IV. These 10 residues are highlighted on the three-dimensional structure of PpcA (Fig. 7). The chemical shift perturbation of the NH group of a single residue Cys^{27} located in the vicinity of heme I most probably represents secondary effects of AQDS binding in the region of heme IV. In fact, previous ^{15}N NMR relaxation experiments carried out on PpcA have shown that Cys^{27} is located in the most flexible region of the polypeptide chain and also shows the highest sensitivity to conformational exchange processes in the microsecond–millisecond time scale [22]. Another strong evidence that further confirms the interaction of AQDS with $PpcA^{ox}$ is the larger chemical shift perturbation observed for heme IV methyl signals (Fig. 5). For the electron transfer between AQDS and $PpcA^{ox}$ to occur at physiologically relevant rates, at least one PpcA heme group and the donor must be in close proximity. Therefore, the larger magnitude observed in the chemical shift perturbation of the heme IV methyl signals compared with that observed in the backbone NH signals indicates that the data is consistent. All three heme groups of PpcA are considerably exposed to the solvent, with heme I showing the largest exposure [22,25]. Therefore, the selective interaction between AQDS and heme IV of $PpcA^{ox}$ must be driven by other factors than simple heme exposure. The location of several lysine residues around heme IV confers a highly positively charged surface near this heme group. Interestingly, the crystal structure of $PpcA^{ox}$ (PDB code 1OS6) showed that the lysine residues located in the vicinity of heme IV form an anion binding region, where two sulfate ions (SO_4^{2-}) were observed [25]. Thus, the two negative charges of AQDS conferred by the two sulfonate ions (see inset on Fig. 1B) are likely to drive AQDS toward heme IV. Therefore, considering the net positive charge of PpcA around heme IV and the negatively charged AQDS, electrostatic interactions are expected to contribute favorably to the binding affinity of the PpcA–AQDS redox complex. In the crystal structure, one sulfate ion is H-bonded to the His^{47} $N_{\delta 1}$ and is close to Lys^{43} (3.4 Å) and Lys^{52} (4.8 Å). Therefore, based on the chemical shift perturbation data, AQDS could bind on the distal site of heme IV between Lys^{43} and Lys^{52}. However, if this is the case it would be expected that the ring of His^{47} will be reoriented, due to the larger volume of AQDS molecule.

Unfortunately, the ring proton signals of the heme axial histidines are extremely broad due to the paramagnetic effect of the unpaired electron of the iron in PpcA^{ox}. Therefore, to probe any change in the geometry of the heme axial ligands, we analyzed the chemical shift perturbation on the βCH_2 protons of all axial ligands of PpcA^{ox} (Supplementary Fig. S3). From this analysis, it is clear that βCH_2 protons of His^{47} are clearly the most affected ones, suggesting a reorientation of His^{47} in presence of AQDS. Moreover, the heme methyl chemical shifts depend on the relative orientation of the heme axial ring planes [46]. Therefore, the larger perturbation observed in the heme IV methyl chemical shifts (Fig. 5B) further confirms the alteration on the geometry of heme IV axial ligands in presence of AQDS. These conclusions are also supported by the docking calculations, which indicate that the complex between PpcA and AH_2QDS is preferably formed near heme IV region (see Fig. 8).

In addition to structural information, the NMR data also provided insights into the binding affinity of the two molecules. The K_d values obtained from the fitting of the ligand-induced chemical shift perturbation curves (Fig. 4) are in the millimolar range and suggest the formation of a low affinity complex. These values are of the same magnitude as those obtained for the binding of calixarene to cytochrome *c* C102T from *Saccharomyces cerevisiae* [47–49]. The low-binding affinity complex and the specific interaction in the proximity of heme IV warrant a rapid and selective electron transfer between the quinone molecule and PpcA, a typical feature in electron transfer reactions between redox partners [40,50,51].

4.1. Implications

This study provides a clear picture of the molecular interaction between PpcA and the humic substance analog AQDS and constitutes an important step toward the rationalization of the *Gs* respiratory chains. Previous structural and thermodynamic studies carried out on PpcA [22,26] showed that the redox behavior of this protein, at physiological pH, involves two dominant microstates: a microstate with hemes I and IV oxidized and the redox-Bohr center deprotonated (P_{14}), and another microstate with heme I oxidized and the redox-Bohr center protonated (P_{1H}) [26]. Since the redox-Bohr center was assigned to one of the propionates of heme IV [21,22], the reduction of heme IV should be coupled to proton transfer at physiological pH. In the present work, NMR experiments showed that the quinone interacts with PpcA^{ox} in the region of heme IV, a feature also supported by docking studies. These results are consistent with the functional mechanism proposed for PpcA (for a review see [26,28]) in which AH_2QDS would transfer electrons and protons to the cytochrome, that could use the energy of the electrons to lower the pK_a of the protons and favor their release in the periplasm. Overall, this process would contribute to the H^+ electrochemical potential gradient across the *Gs* periplasmic membrane that drives ATP synthesis. This functional mechanism would be compatible with the observation made by Coates et al., 2002 [18], who showed that species of *Geobacteraceae*, among others, can convert AH_2QDS to AQDS during growth without affecting the anthraquinone concentration, indicating that AH_2QDS is not degraded as a carbon source by these organisms, but simply oxidized as energy source.

This work also shows that the interaction between the two redox partners is productive, leading to electron transfer. From the UV–visible and stopped-flow studies it could be concluded that the extent of the electron transfer is under thermodynamic control, i.e. it is more favorable from the reduced quinone to the oxidized PpcA, than in the opposite direction. However, the observed rates measured by the stopped-flow technique, are fast and very similar for both reactions (reductive and oxidative). Consequently, despite the thermodynamic preference for the use of reduced AH_2QDS as electron donor, when compared to the use of oxidized AQDS as electron acceptor, the fast kinetics observed in both directions make the two processes physiologically feasible, as long as the diffusion and regeneration of the quinone molecules is compatible with the flow of electrons through the metabolism of the organism. We may conclude that *Gs* can live utilizing AH_2QDS as an energy source and carbon from other limited but readily degradable source, or use reduced carbon as a source of carbon and energy and utilize AQDS as terminal electron acceptor, depending on what is available in the environment.

Acknowledgements

We would like to thank to Dr. Marianne Schiffer for helpful discussion. This work was supported by project grant PTDC/BBB-BEP/0753/2012 (to CAS), the strategic grant PEst-C/EQB/LA0006/2013 (to REQUIMTE Laboratório Associado) and the re-equipment grant REEQ/336/BIO/2005 from the Fundação para a Ciência e a Tecnologia (FCT), Portugal. The NMR spectrometers are part of The National NMR Facility, supported by FCT, Portugal (RECI/BBB-BQB/0230/2012). JMD is the recipient of grant SFRH/BD/89701/2012 from FCT. PRP is partially supported and OK is fully supported by the Division of Chemical Sciences, Geosciences, and Biosciences, Office of Basic Energy Sciences of the U.S. Department of Energy program under contract no. DE-AC02-06CH11357. The authors thank the anonymous referees for the valuable comments and constructive suggestions that helped them to improve the paper.

Appendix A. Supplementary data

Supplementary data to this article can be found online at http://dx.doi.org/10.1016/j.bbabio.2014.02.004.

References

[1] R. Mahadevan, B.O. Palsson, D.R. Lovley, In situ to *in silico* and back: elucidating the physiology and ecology of *Geobacter* spp. using genome-scale modelling, Nat. Rev. Microbiol. 9 (2011) 39–50.
[2] D.R. Bond, D.R. Lovley, Electricity production by *Geobacter sulfurreducens* attached to electrodes, Appl. Environ. Microbiol. 69 (2003) 1548–1555.
[3] D.R. Lovley, D.E. Holmes, K.P. Nevin, Dissimilatory Fe(III) and Mn(IV) reduction, Adv. Microb. Physiol. 49 (2004) 219–286.
[4] D.R. Lovley, Extracellular electron transfer: wires, capacitors, iron lungs, and more, Geobiology 6 (2008) 225–231.
[5] R.T. Anderson, H.A. Vrionis, I. Ortiz-Bernad, et al., Stimulating the in situ activity of *Geobacter* species to remove uranium from the groundwater of a uranium-contaminated aquifer, Appl. Environ. Microbiol. 69 (2003) 5884–5891.
[6] K.B. Gregory, D.R. Lovley, Remediation and recovery of uranium from contaminated subsurface environments with electrodes, Environ. Sci. Technol. 39 (2005) 8943–8947.
[7] J.R. Lloyd, D.R. Lovley, Microbial detoxification of metals and radionuclides, Curr. Opin. Biotechnol. 12 (2001) 248–253.
[8] K.A. Weber, L.A. Achenbach, J.D. Coates, Microorganisms pumping iron: anaerobic microbial iron oxidation and reduction, Nat. Rev. Microbiol. 4 (2006) 752–764.
[9] K.T. Finneran, M.E. Housewright, D.R. Lovley, Multiple influences of nitrate on uranium solubility during bioremediation of uranium-contaminated subsurface sediments, Environ. Microbiol. 4 (2002) 510–516.
[10] D.R. Lovley, J.D. Coates, E.L. Blunt-Harris, et al., Humic substances as electron acceptors for microbial respiration, Nat. (Lett.) 382 (1996) 445–447.
[11] Z. Struyk, G. Sposito, Redox properties of standard humic acids, Geoderma 102 (2001) 329–346.
[12] D.R. Lovley, J.L. Fraga, J.D. Coates, et al., Humics as an electron donor for anaerobic respiration, Environ. Microbiol. 1 (1999) 89–98.
[13] S.M. Strycharz, R.H. Glaven, M.V. Coppi, et al., Gene expression and deletion analysis of mechanisms for electron transfer from electrodes to *Geobacter sulfurreducens*, Bioelectrochemistry 80 (2011) 142–150.
[14] J.D. Coates, D.J. Ellis, E.L. Blunt-Harris, et al., Recovery of humic-reducing bacteria from a diversity of environments, Appl. Environ. Microbiol. 64 (1998) 1504–1509.
[15] J.W. Voordeckers, B.C. Kim, M. Izallalen, et al., Role of *Geobacter sulfurreducens* outer surface *c*-type cytochromes in reduction of soil humic acid and anthraquinone-2,6-disulfonate, Appl. Environ. Microbiol. 76 (2010) 2371–2375.
[16] D.R. Lovley, J.L. Fraga, E.L. Blunt-Harris, et al., Humic substances as a mediator for microbially catalyzed metal reduction, Acta Hydrochim. Hydrobiol. 26 (1998) 152–157.
[17] F. Aulenta, V.D. Maio, T. Ferri, et al., The humic acid analogue antraquinone-2,6-disulfonate (AQDS) serves as an electron shuttle in the electricity-driven microbial dechlorination of trichloroethene to cis-dichloroethene, Bioresour. Technol. 101 (2010) 9728–9733.
[18] J.D. Coates, K.A. Cole, R. Chakraborty, et al., Diversity and ubiquity of bacteria capable of utilizing humic substances as electron donors for anaerobic respiration, Appl. Environ. Microbiol. 68 (2002) 2445–2452.

[19] B.A. Methé, K.E. Nelson, J.A. Eisen, et al., Genome of *Geobacter sulfurreducens*: metal reduction in subsurface environments, Science 302 (2003) 1967–1969.
[20] J.R. Lloyd, C. Leang, A.L. Hodges Myerson, et al., Biochemical and genetic characterization of PpcA, a periplasmic *c*-type cytochrome in *Geobacter sulfurreducens*, Biochem. J. 369 (2003) 153–161.
[21] L. Morgado, M. Bruix, V. Orshonsky, et al., Structural insights into the modulation of the redox properties of two *Geobacter sulfurreducens* homologous triheme cytochromes, Biochim. Biophys. Acta 1777 (2008) 1157–1165.
[22] L. Morgado, V.B. Paixão, M. Schiffer, et al., Revealing the structural origin of the redox-Bohr effect: the first solution structure of a cytochrome from *Geobacter sulfurreducens*, Biochem. J. 441 (2012) 179–187.
[23] M. Pessanha, Y.Y. Londer, W.C. Long, et al., Redox characterization of *Geobacter sulfurreducens* cytochrome c_7: physiological relevance of the conserved residue F15 probed by site-specific mutagenesis, Biochemistry 43 (2004) 9909–9917.
[24] M. Pessanha, L. Morgado, R.O. Louro, et al., Thermodynamic characterization of triheme cytochrome PpcA from *Geobacter sulfurreducens*: evidence for a role played in e^-/H^+ energy transduction, Biochemistry 45 (2006) 13910–13917.
[25] P.R. Pokkuluri, Y.Y. Londer, N.E. Duke, et al., Family of cytochrome c_7-type proteins from *Geobacter sulfurreducens*: structure of one cytochrome c_7 at 1.45 Å resolution, Biochemistry 43 (2004) 849–859.
[26] L. Morgado, M. Bruix, M. Pessanha, et al., Thermodynamic characterization of a triheme cytochrome family from *Geobacter sulfurreducens* reveals mechanistic and functional diversity, Biophys. J. 99 (2010) 293–301.
[27] P.R. Pokkuluri, Y.Y. Londer, X. Yang, et al., Structural characterization of a family of cytochromes c_7 involved in Fe(III) respiration by *Geobacter sulfurreducens*, Biochim. Biophys. Acta 1797 (2010) 222–232.
[28] L. Morgado, J.M. Dantas, M. Bruix, et al., Fine tuning of redox networks on multiheme cytochromes from *Geobacter sulfurreducens* drives physiological electron/proton energy transduction, Bioinorg. Chem. Appl. 2012 (2012) 1-9.
[29] J.B. Shyu, D.P. Lies, D.K. Newman, Protective role of *tolC* in efflux of the electron shuttle anthraquinone-2,6-disulfonate, J. Bacteriol. 184 (2002) 1806–1810.
[30] A.P. Fernandes, I. Couto, L. Morgado, et al., Isotopic labeling of *c*-type multiheme cytochromes overexpressed in *E. coli*, Protein Expr. Purif. 59 (2008) 182–188.
[31] E. Arslan, H. Schulz, R. Zufferey, et al., Overproduction of the *Bradyrhizobium japonicum c*-type cytochrome subunits of the cbb_3 oxidase in *Escherichia coli*, Biochem. Biophys. Res. Commun. 251 (1998) 744–747.
[32] Y.Y. Londer, P.R. Pokkuluri, D.M. Tiede, et al., Production and preliminary characterization of a recombinant triheme cytochrome c_7 from *Geobacter sulfurreducens* in *Escherichia coli*, Biochim. Biophys. Acta 1554 (2002) 202–211.
[33] S. Seeliger, R. Cord-Ruwisch, B. Schink, A periplasmic and extracellular *c*-type \cytochrome of *Geobacter sulfurreducens* acts as a ferric iron reductase and as an electron carrier to other acceptors or to partner bacteria, J. Bacteriol. 180 (1998) 3686–3691.
[34] M. Dixon, The acceptor specificity of flavins and flavoproteins. I. Techniques for anaerobic spectrophotometry, Biochim. Biophys. Acta Bioenerg. 226 (1971) 241–258.
[35] D.S. Wishart, C.G. Bigam, A. Holm, et al., 1H, 13C and 15 N random coil NMR chemical shifts of the common amino acids. I. Investigations of nearest-neighbor effects, J. Biomol. NMR 5 (1995) 67–81.
[36] L. Morgado, A.P. Fernandes, Y.Y. Londer, et al., One simple step in the identification of the cofactors signals, one giant leap for the solution structure determination of multiheme proteins, Biochem. Biophys. Res. Commun. 393 (2010) 466–470.
[37] F.H. Schumann, H. Riepl, T. Maurer, et al., Combined chemical shift changes and amino acid specific chemical shift mapping of protein–protein interactions, J. Biomol. NMR 39 (2007) 275–289.
[38] P.T. Lang, S.R. Brozell, S. Mukherjee, et al., DOCK 6: combining techniques to model RNA-small molecule complexes, RNA 15 (2009) 1219–1230.
[39] E.F. Pettersen, T.D. Goddard, C.C. Huang, et al., UCSF Chimera — a visualization system for exploratory research and analysis, J. Comput. Chem. 25 (2004) 1605–1612.
[40] M. Prudêncio, M. Ubbink, Transient complexes of redox proteins: structural and dynamic details from NMR studies, J. Mol. Recognit. 17 (2004) 524–539.
[41] F. Meschi, F. Wiertz, L. Klauss, et al., Efficient electron transfer in a protein network lacking specific interactions, J. Am. Chem. Soc. 133 (2011) 16861–16867.
[42] K. Sakamoto, M. Kamiya, M. Imai, et al., NMR basis for interprotein electron transfer gating between cytochrome *c* and cytochrome c oxidase, Proc. Natl. Acad. Sci. U. S. A. 108 (2011) 12271–12276.
[43] N. Yahata, T. Saitoh, Y. Takayama, et al., Redox interaction of cytochrome c(3) with [NiFe] hydrogenase from *Desulfovibrio vulgaris* Miyazaki F, Biochemistry 45 (2006) 1653–1662.
[44] Y.H. Ding, K.K. Hixson, M.A. Aklujkar, et al., Proteome of *Geobacter sulfurreducens* grown with Fe(III) oxide or Fe(III) citrate as the electron acceptor, Biochim. Biophys. Acta 1784 (2008) 1935–1941.
[45] W.M. Clark, Oxidation–reduction potentials of organic systems, Williams & Wilkins, 1960.
[46] D.L. Turner, C.A. Salgueiro, P. Schenkels, et al., Carbon-13 NMR studies of the influence of axial ligand orientation on haem electronic structure, Biochim. Biophys. Acta 1246 (1995) 24–28.
[47] R.E. McGovern, H. Fernandes, A.R. Khan, et al., Protein camouflage in cytochrome *c*-calixarene complexes, Nat. Chem. 4 (2012) 527–533.
[48] S. Gordo, V. Martos, E. Santos, et al., Stability and structural recovery of the tetramerization domain of p53-R337H mutant induced by a designed templating ligand, Proc. Natl. Acad. Sci. U. S. A. 105 (2008) 16426–16431.
[49] V. Martos, S.C. Bell, E. Santos, et al., Molecular recognition and self-assembly special feature: calix[4]arene-based conical-shaped ligands for voltage-dependent potassium channels, Proc. Natl. Acad. Sci. U. S. A. 106 (2009) 10482–10486.
[50] M. Ubbink, Complexes of photosynthetic redox proteins studied by NMR, Photosynth. Res. 81 (2004) 277–287.
[51] Q. Bashir, S. Scanu, M. Ubbink, Dynamics in electron transfer protein complexes, FEBS J. 278 (2011) 1391–1400.
[52] K.R. Cousins, Computer review of ChemDraw Ultra 12.0, J. Am. Chem. Soc. 133 (2011) 8388.
[53] G.P. Moss, Nomenclature of tetrapyrroles. Recommendations 1986 IUPAC-IUB Joint Commission on Biochemical Nomenclature (JCBN), Eur. J. Biochem. 178 (1988) 277–328.
[54] W.L. DeLano, The PyMOL Molecular Graphics System, 2002, on World Wide Web, 2002. http://www.pymol.org.